High-speed three-dimensional shape measurement for dynamic scenes using bi-frequency tripolar pulse-width-modulation fringe projection

Chao Zuo [a,b,*], Qian Chen [a,b], Guohua Gu [a], Shijie Feng [a], Fangxiaoyu Feng [a], Rubin Li [a], Guochen Shen [a]

[a] Jiangsu Key Laboratory of Spectral Imaging & Intelligence Sense, Nanjing University of Science and Technology, Nanjing, Jiangsu Province 210094, China
[b] Key Laboratory of Photoelectronic Imaging Technology and System, Ministry of Education of China, Beijing Institute of Technology, Beijing 100081, China

ABSTRACT

This paper introduces a high-speed three-dimensional (3-D) shape measurement technique for dynamic scenes by using bi-frequency tripolar pulse-width-modulation (TPWM) fringe projection. Two wrapped phase maps with different wavelengths can be obtained simultaneously by our bi-frequency phase-shifting algorithm. Then the two phase maps are unwrapped using a simple look-up-table based number-theoretical approach. To guarantee the robustness of phase unwrapping as well as the high sinusoidality of projected patterns, TPWM technique is employed to generate ideal fringe patterns with slight defocus. We detailed our technique, including its principle, pattern design, and system setup. Several experiments on dynamic scenes were performed, verifying that our method can achieve a speed of 1250 frames per second for fast, dense, and accurate 3-D measurements.

Crown Copyright © 2013 Published by Elsevier Ltd. All rights reserved.

1. Introduction

The three-dimensional (3-D) scene acquisition is becoming increasingly crucial in practical application fields such as machine design, industrial inspection, prototyping, machine vision, robotics, 3-D imaging, game industry, culture heritage protection, advertising, information exchange and other fields of modern information technologies [1]. Fringe projection methods have been considered one of the most reliable techniques for recovering the shape of objects because of their accuracy and efficiency [2]. Recent advance in image sensors and digital projection technology becomes a powerful vehicle that motivates the rapid progress in reconstructing the 3-D shapes of dynamic scenes such as high-speed moving objects and rotating or vibrating non-rigid bodies [3,4]. High-speed 3-D dynamic shape measurement is essential and can be widely applied in such application fields as biomedical investigation, fluid dynamics, solid mechanics, deformation analysis under stress, impact and tension, where precise, accurate high-speed recordings are a must [3–8]. It is desirable that the 3-D information can be acquired at such a high speed that the details of shape changes in an instant can be captured, which can provide in-depth visual insights into events that happen during accidents [9].

Over the years, a number of fringe projection techniques have been developed by modifying the off-the-shelf digital projectors for high-speed applications [10–13]. Considering the resolution and the accuracy of measurements, most of these techniques use multiply sequentially sinusoidal patterns. In order to reliably determine the range information at each position, the scene must be almost static while each frame of the pattern is projected. However, most digital light processing (DLP) projectors are only capable of projecting patterns at a rate of 120 frames per second (fps) [4]. So it is difficult to use these projectors to capture fast moving dynamic scenes. On the other hand, today's high-speed camera, although relatively expensive, have a much higher frame rate (kHz) with a sufficient image resolution for most applications. To match the high recording speed of the camera, some researchers employed the DLP Discovery kit to control and program each mirror in the digital micromirror device (DMD) at a rather high speed so that the incident illumination could be precisely controlled [5,7,14,15]. However, since the DMD is a binary digital device: the DMD mirrors can be just switched between two orientations. In one orientation, incident light is reflected by the mirror toward the outside scene and in the other, light is reflected onto a black surface within the projector. This means only two illumination intensities can be generated at one moment within one switching cycle of DMD. To generate a gray-scale sinusoidal pattern, it must integral the illumination by

---

binary temporal pulse width modulation [5,16], and the intensity level is reproduced by controlling the amount of time the mirror is on/off. For example, a 1-bit binary image just need one working cycles while an 8-bit gray-scales image needs 256 working cycles. So it is preferable that the pattern can be generated using as fewer gray-scales as possible so that it can be reproduced by DMD at a higher switching speed. For this purpose, Lei and Zhang [17] proposed a technique called squared binary defocusing method (SBM) that is to generate sinusoidal fringe patterns by properly defocusing squared binary structured ones. Ayubi et al. [18] presented methods for generating the binary pattern by the sinusoidal pulse-width-modulation (SPWM) technique of electrical engineering. Wang and Zhang proposed a binary pattern generation technique called optimal pulse-width-modulation (OPWM) [14] and conducted a comparative study on SBM, SPWM, and OPWM [19]. With these binary defocused patterns, the dynamic 3-D shape measurement can be achieved using either phase-shifting profilometry or Fourier transform profilometry. However, the boost in projection speed has been accompanied by a number of challenging issues: (1) The contradiction between the measurement accuracy with depth of field of the measurement: although SPWM and OPWM method can greatly improve the sinusoidality of the binary pattern, when the defocusing level is insufficient or the projector is nearly focused, the phase error caused by some unwanted high order harmonics of the generated patterns of SPWM and OPWM methods is still nonnegligible [16]. Conversely, an ideal sinusoidal pattern can be generated with a larger degree of defocusing, while the pattern contrast will be reduced by the effect of defocus. Therefore the close-to-be-ideally sinusoidal fringe pattern can be generated within a small depth range. (2) Efficient high-speed multi-object measurement: For measuring multiple objects simultaneously, the absolute phase should be recovered without ambiguity. To achieve this, Wang and Zhang [20] proposed a superfast phase-shifting technique for 3-D measurement using defocused binary patterns. Combining with the multi-frequency temporal unwrapping [21] and Gray-coding [15], the phase ambiguity problem can be solved. However, to unwrap a high-frequency phase, the minimum number of binary patterns is $INT(\log_2 F) + 1$, where F is the total number of periods in the field and INT is the 'integer part' function [22]. Besides, the phase unwrapping will easily fall into an error, when an improper value of Gray-coding is caused by mistake at the partial boundary of two adjacent binary words [15,23]. Temporal phase unwrapping is a well-established technique to retrieve the absolute phase [24,25]. However, at least six frames are needed for a two-frequency unwrapping and nine frames are needed for a three frequency method. Due to the relatedly higher phase error of the defocus pattern, usually a three frequency method is mandatory [21]. Obviously, the increased number of required patterns is undesirable under dynamic conditions, where it is preferable to minimize acquisition time to avoid the effect of motion.

The goal of this research is to present a new three-dimensional shape measurement technique for dynamic scenes combining our recently proposed Tripolar pulse-width-modulation (TPWM) [16] pattern strategy with a new bi-frequency phase-shifting algorithm. As we recently reported, the TPWM technique can generate ideal sinusoidal fringe pattern even with a nearly focused optical system, which greatly increases the measurement accuracy and depth range of the defocusing method. The newly introduced bi-frequency phase-shifting algorithm can retrieve two phase maps with different fringe frequencies with only five fringe images. By applying a number-theoretical phase-unwrapping, the absolute phase can be easily obtained by a look-up table (LUT) based implementation. We discuss three typical methods for two-frequency phase-unwrapping, and explained the advantages of

the adopted number-theoretical phase-unwrapping for our defocusing TPWM pattern. We also discuss the design of TPWM pattern as well as the synchronization between the projector and the high-speed camera. Experiments on two dynamic scenes are preformed to verify the performance of the proposed technique.

2. Bi-frequency tripolar pulse-width-modulation fringe projection

In this section, we detail our technique in three aspects: first, we introduce the bi-frequency phase-shifting method in which two different wrapped phase maps can be obtained by analyzing only five fringe images. Then we review three most widely used two-frequency phase-unwrapping algorithms. Finally, we briefly introduce the TPWM pattern generation technique and explain the advantages and necessity of combining the number-theoretical phase-unwrapping with TPWM technique.

2.1. Bi-frequency phase-shifting method

Phase-shifting profilometry has become one of the most popular phase extraction approaches, because it completely eliminates interferences from ambient light and surface reflectivity. Requiring the least number of fringe patterns for 3-D shape recovery, the three-step phase-shifting algorithm has been used extensively in high-speed applications [4]. The fringe images of a three-step phase-shifting algorithm with equal phase-shift can be described as

$$I_1(x,y) = A(x,y) + B(x,y)\cos(\phi_1 - 2\pi/3), \tag{1}$$

$$I_2(x,y) = A(x,y) + B(x,y)\cos(\phi_1), \tag{2}$$

$$I_3(x,y) = A(x,y) + B(x,y)\cos(\phi_1 + 2\pi/3), \tag{3}$$

where $A(x,y)$ is the average intensity relating to the pattern brightness and background illumination, $B(x,y)$ is the intensity modulation relating to the pattern contrast and surface reflectivity. ϕ_1 is the corresponding wrapped phase map which can be extracted by the following equation:

$$\phi_1(x,y) = \tan^{-1}(\sqrt{3}(I_1 - I_3)/(2I_2 - I_1 - I_3)). \tag{4}$$

Since the arctangent function only ranges from $-\pi$ to π, the phase value provided from Eq. (4) will have π phase discontinuities. To obtain an absolute phase distribution, a phase unwrapping algorithm is usually needed. The absolute phase distribution is necessary for 3-D shape measurement of isolated objects with complex shapes. Spatial phase unwrapping algorithms cannot resolve the phase ambiguity in discontinuous surfaces and large step height changes where the phase changes large than π [26]. In order to obtain the reliable absolute phase distribution of a deformed fringe pattern, another set of two fringe images with π phase-shift (the fringe pitch is different from $I_1 - I_3$) are used

$$I_4(x,y) = A(x,y) + B(x,y)\sin(\phi_2), \tag{5}$$

$$I_5(x,y) = A(x,y) + B(x,y)\cos(\phi_2) \tag{6}$$

Assuming that both the camera and the projector have a fairly large depth-of-view and the reflection of the object surface is linear, the average intensity coefficients $A(x,y)$ should be constant for pixel (i, j) in all the five images. It can be calculated using the

following equation:

$$A(x,y) = (I_1(x,y) + I_2(x,y) + I_3(x,y))/3. \tag{7}$$

Utilizing the $A(x,y)$ obtained, another wrapped phase map ϕ_2 can be computed as follows:

$$\phi_2(x,y) = \tan^{-1}((I_4 - A)/(I_5 - A)) \tag{8}$$

By now we have obtained two wrapped phase maps: ϕ_1 and ϕ_2 by using only five fringe patterns. Note ϕ_2 is different from ϕ_1 when the fringe frequency of I_4 and I_5 is not equal to that of $I_1 - I_3$, which is exactly what we wanted because they provided extra information to carry out the phase unwrapping, so that the absolute phase map for isolated objects or object containing sharp height variations can be recovered. Notice that although assumed to be a constant for all five images, $B(x,y)$ is not utilized to further reduce the number of patterns required in phase map construction. This is because, in practice the value of $B(x,y)$ may vary slightly for fringe patterns with different wavelengths due to the out-of-focus projection on the object's surface. However, this does not affect the value of $A(x,y)$ at all.

2.2. Absolute phase map recovery

As stated before, the wrapped phases ϕ_1 and ϕ_2 obtained by Eqs. (4) and (8) range from $-\pi$ to π. Retrieving the absolute phase maps Φ_1 or Φ_2 from the wrapped ones, ϕ_1 and ϕ_2, we have

$$\begin{cases} \Phi_1(x,y) = \phi_1(x,y) + 2\pi k_1(x,y) \\ \Phi_2(x,y) = \phi_2(x,y) + 2\pi k_2(x,y) \end{cases}. \tag{9}$$

and they should have the following relationship:

$$\Phi_1(x,y) = (\lambda_2/\lambda_1)\Phi_2(x,y), \tag{10}$$

where the λ_1 and λ_2 stands for the wavelengths of the pattern I_1–I_3 and I_4–I_5, respectively. The $k_i(x,y)$, $i = 1, 2$ in Eq. (9) is the fringe order to represent phase jumps. The key task for the absolute phase map recovery is quickly and correctly determining $k_i(x,y)$ for each pixel in the phase map. To eliminate ambiguity in assignment of unwrapped fringe order, a straightforward method is to obtain a low-resolution phase with a set of unit frequency patterns (e.g. λ_2 is large enough to cover the view of the camera) so that the calculated phase (e.g. $\phi_2(x,y)$) has a range of less than 2π [24,25]. In this case, no phase unwrapping is required for $\phi_2(x,y)$, i.e. $\Phi_2(x,y) = \phi_2(x,y)$. Combining Eqs. (9) and (10), we can obtain $k_1(x,y)$ for each pixel easily. By this means the phase $\phi_1(x,y)$ at higher spatial frequency can be successfully unwrapped. Here we refer this method *reduced hierarchical approach*.

An alternate approach so-called *phase-difference approach* [27–29] is to generate a low-frequency phase by subtracting two higher frequency phase maps with different pitches. The low-frequency phase (phase difference) will give low-frequency information enables unwrapping the high-frequency phase so that the unambiguous measurement range is increased. If the initial two phase maps are acquired at wavelengths λ_1 and λ_2, their phase difference is therefore

$$\Delta\phi_{12}(x,y) = (\phi_1(x,y) - \phi_2(x,y)) \bmod 2\pi. \tag{11}$$

The equivalent wavelength of $\Delta\phi_{12}(x, y)$ is [27]

$$\lambda_{12} = \lambda_1\lambda_2/(\lambda_2 - \lambda_1). \tag{12}$$

We call λ_{12} the "synthetic wavelength". If $\lambda_1 < \lambda_2 < 2\lambda_1$, we have $\lambda_1 < \lambda_2 < \lambda_{12}$. When λ_1 and λ_2 are properly chosen and spaced closely, the synthetic wavelength can be large enough so that the phase ambiguity can be removed. The fringe order at λ_i, $i = 1, 2$ is determined by scaling the phase difference $\Delta\phi_{12}(x, y)$ by a factor of λ_{12}/λ_i, $i = 1, 2$ and subtracting the phase $\Delta\phi_i$, $i = 1, 2$.

The final method we will mention is the number-theoretical approach [28–34], which is based on the properties of relative prime numbers. The core of the number-theoretical approach relies on the fact that for suitable chosen wavelength lengths λ_1 and λ_2, one can obtain a unique set of pairs (ϕ_1, ϕ_2) along the absolute phase axis. "Suitable" means that the pattern wavelengths have to unconditionally be relative primes to produce any kind of usable output. When this is the case, a product of pattern wavelengths $\lambda_1\lambda_2$ determines the range on the absolute phase axis within which we acquire the unique pairs for wrapped phase values. This originates from number theory and the divisibility properties of integers [35]. For simplicity of explanation, we consider an example with $\lambda_1 = 3$ pixels and $\lambda_2 = 5$ pixels. Fig. 1 shows changes of two wrapped phase maps along the absolute phase axis where the first wrapped phase map has $\lambda_1 = 3$ pixels and the second has $\lambda_2 = 5$ pixels. Therefore, the unambiguous range is 15 pixels. Careful observation reveals that certain intervals on the absolute phase axis are characterized by unique pairs of (k_1, k_2). Examining their wrapped phase maps, it can be found that each pair of wrapped phase maps are unique, therefore the fringe order of the two unwrapped phase maps can be determined by examining their wrapped phases.

Besides, the number-theoretical method can successfully cope even with sets of wavelengths which are not necessarily relative primes. More specifically, it correctly unwraps the phase up to the value in the absolute phase which equals to LCM(λ_1, λ_2) [32]. Here LCM () represents a function whose output is the least common multiple for input parameters, which is a minimal number divisible by the wavelengths used. It should be plain to see that in cases where wavelengths are prime numbers, then the LCM () function simply boils down to multiplication of the lengths. In other cases, we simply rely on an efficient Euclid algorithm to compute the greatest common divisor GDC(λ_1, λ_2) and ultimately compute LCM(λ_1, λ_2) = $\lambda_1\lambda_2$/GDC(λ_1, λ_2) [35]. To determine the two integers k_1 and k_2 via the two unwrapped phase maps, we rewrite Eq. (10) as
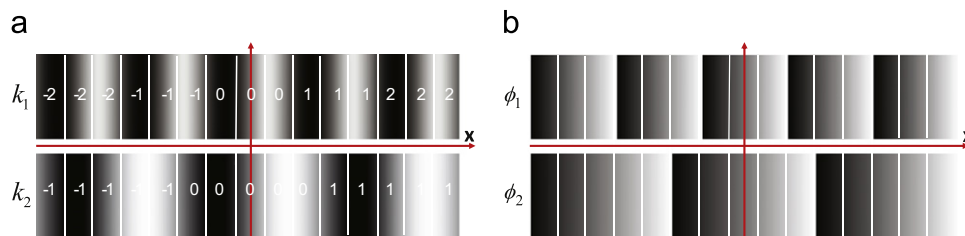
$$p_2\Phi_1(x,y) = p_1\Phi_2(x,y), \tag{13}$$

Fig. 1. Number-theoretical phase unwrapping for two wavelengths of 3 and 5 pixels. Each rectangle separated by vertical white lines represents one pixel. (a) The appearance of two sine patterns with the fringe orders. (b) The pairs of wrapped phase maps, every combination is unique.

where p_i ($i = 1, 2$) stands for the total number of fringes for their corresponding patterns within the unambiguous range and we have $p_i = LCM(\lambda_1, \lambda_2)/\lambda_i$. Combining Eqs. (13) and (9) yields:

$$(p_1\phi_2 - p_2\phi_1)/2\pi = k_2 p_1 - k_1 p_2. \tag{14}$$

Generally, the wavelength should be integers (in pixels), so the right hand side of Eq. (14) is an integer. Therefore, the left-hand side must also be the same integer. We can use the values of the left-hand side as the entries to determine these two integers uniquely [33,34]. In order to speed up data processing, all these unique map pairs of (k_1, k_2) can be pre-computed and the results can be stored in a look-up-table (LUT). When the two phase maps at a given position are obtained, we calculate their weighted difference $(p_2\phi_1 - p_1\phi_2)/2\pi$, round its value to the closest integer, and then use the pre-computed LUT to determine the fringe order pair. Once the (k_1, k_2) is obtained, the absolute phase can be obtained using Eq. (9).

We still use the above example to illustrate how the LUT can be built. The value of $(3\phi_1 - 5\phi_2)/2\pi$ are plotted in Fig. 2 from which it is easily observed that there is a one-to-one relationship between the (k_1, k_2) and the value of $(3\phi_1 - 5\phi_2)/2\pi$. The final LUT build is shown in Table 1.

2.3. Pattern generation using tripolar pulse-width-modulation

Combining bi-frequency phase-shifting method with the two-frequency absolute phase map recovery method, we can obtain
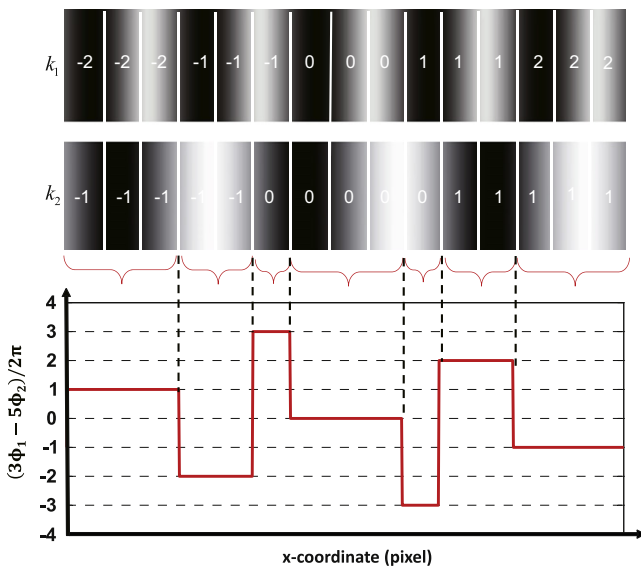

Fig. 2. Number-theoretical phase unwrapping for two-wavelengths of 3 and 5 pixels. Using values of $(3\phi_1 - 5\phi_2)/2\pi$, we can determine fringe order pairs (k_1, k_2) without ambiguity.

Table 1
The LUT of number-theoretical phase unwrapping for two-wavelengths of 3 and 5 pixels.

$(3\phi_1 - 5\phi_2)/2\pi$	k_1	k_2
−3	1	0
−2	−1	−1
−1	2	1
0	0	0
1	−2	−1
2	1	1
3	−1	0

the absolute phase with the phase ambiguity eliminated. Although there are only five frames used to recover the two-frequency phase maps, they must be projected sequentially onto the tested objects. In order to determine the phase value at each position, the scene must be almost static while each frame of the pattern is projected. Since most commercial DLP projectors are only capable of projecting patterns at a rate of 120 fps, it is difficult to use these projectors to capture fast moving dynamic scenes.

The key factor which restricts the speed of the DLP projector is the working mechanism of its key component DMD. The DMD in a DLP projector is capable of switching mirrors "on" and "off" at high speeds (tens of kHz). An off-the-shelf DLP projector, however, effectively operates at much lower rates (60–120 Hz) by integrating smaller binary intensities over time by a sensor (eye or camera) to produce the desired intensity value. By reducing the gray-scales of the projected pattern, as well as the recently developed DLP Discovery technology, the pattern switching rate can be improved significantly. For example, the DLP Discovery 4100 can switch images at faster than 32 kHz for 1-bit binary patterns, which typically exceeds the speed of a state-of-the-art high-speed camera with decent resolution and quality. So employing only very few gray-scales (two or three), which is preferable for increasing the rate of pattern projection. However, decrease in the gray-scales of the projected pattern inevitably results in deterioration of its sinusoidality. It's not difficult to understand that with the current resolution of the DMD, it is impossible to preferably emulate a *unit-frequency* sinusoidal pattern with only two or three gray-scales, even with a highly defocused optical system. So it is impractical to use reduced hierarchical approach for absolute phase recovery in our technique.

Compared with the phase-difference approach, the number-theoretical approach enjoys larger unambiguous ranges (generally, $LCM(\lambda_1, \lambda_2) \geq \lambda_{12}$) and greater flexibilities in choosing the fringe wavelengths, so it is the most suitable solution for absolute phase recovery using our bi-frequency phase-shifting method. However, in practice, there are many factors such as nonsinusoidality of the pattern intensity, random noise of the projector and the camera may induce errors in obtained wrapped phase maps. These problems are even worse for high-speed applications with limited exposure time and defocused patterns. Generally, the phase error caused by nonsinusoidal pattern is usually greater than that random noise. The phase error is closely related to the (1) the spectrum/harmonics of the fringe pattern; (2) the sensitivity to harmonics of the phase-shifting algorithm. Eq. (4) is the three-step phase-shifting algorithm, so it is insensitive to triplen harmonics, whilst Eq. (8) can be viewed as a modified two-plus-one phase-shifting algorithm and it has no anti-harmonics ability. From the simulation results in [16], we know that the maximal phase error may exceed 0.5 rad for SBM pattern or 0.3 rad for SPWM pattern when the projector is slightly defocused (equivalent to the effect of a Gaussian filter with a standard deviation of 1.5 pixels). However, from [34] we know if the maximal phase error is larger than $\pi/(p_1 + p_2)$, mistakes will occur in determining the fringe orders. So we must guarantee that the relationship $p_1 + p_2 < \pi/\Delta\phi_{max}$ can be established. It can be deduced that for SPWM pattern, the total number of fringes within the unambiguous range is limited to less than 10 and for SBM pattern, the number is limited to less than 6, which is of course inadequate for high accurate measurements. Furthermore, if the other error sources are considered, the measurement range will be reduced more.

To further reduce the higher-order harmonics and improve the sinusoidality of the defocused pattern, we proposed a new pattern generation technique called TPWM [16], in which the undesired harmonics can be displaced so far away from the fundamental

frequency that close-to-ideal sinusoidal patterns can be generated with very small defocusing level. Fig. 3 shows an example of TPWM pattern with $f_c = 10f_0$, where f_c and f_0 stand for the frequency of triangular carrier and the sinusoidal waveform, respectively. The TPWM waveform is generated by comparing two high-frequency triangular carrier displaced by π shift with the desired sinusoidal waveform. Fig. 3(c) shows the spectrum of the TPWM waveform. It can be observed that the spectrum of the TPWM pattern has peaks around the frequency $2f_c$, so they can be easily suppressed even with a nearly focused optical system, and thus an quasi-ideal sinusoidal pattern can be obtained.

From the simulation results in [16], we know that the maximal phase error $\Delta\phi_{max}$ of TPWM is *always* less than 0.1 rad for phase-shifting algorithms with *any* steps due to the high sinusoidality of the TPWM pattern. That means the unambiguous range and the maximum number of fringe could be processed can be greatly improved.

It is also important to note that the TPWM pattern utilizes one more gray-scales than the binary ones, which means it needs two switching cycles of DMD to synthesize one TPWM pattern, reducing the maximal pattern projection speed to half. But this also enables prolonging the exposure time of the camera to improve the image quality. On the other hand, the DLP Discovery technology can switch images at faster than 16 kHz for ternary patterns; this frame rate is enough for most applications.
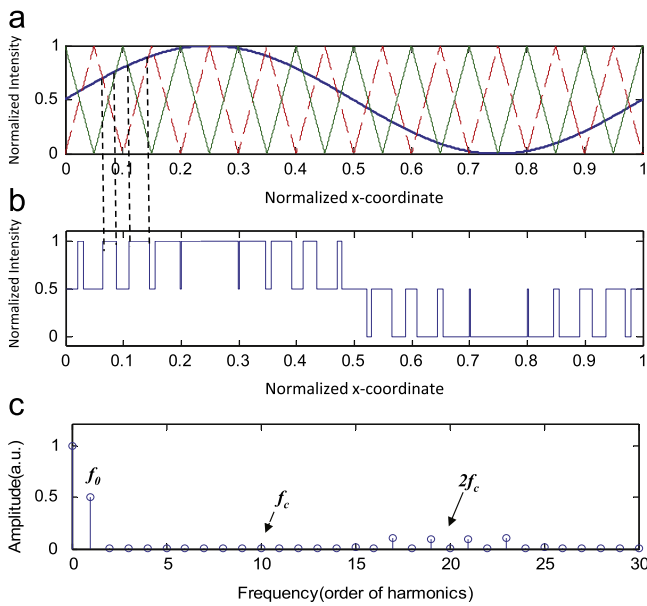

Fig. 3. TPWM waveform generation and harmonics distribution. (a) The sinusoidal and the two modulation triangle waveforms displaced by π ($f_c = 10f_0$); (b) the resultant TPWM pattern; (c) frequency spectrum of (b).
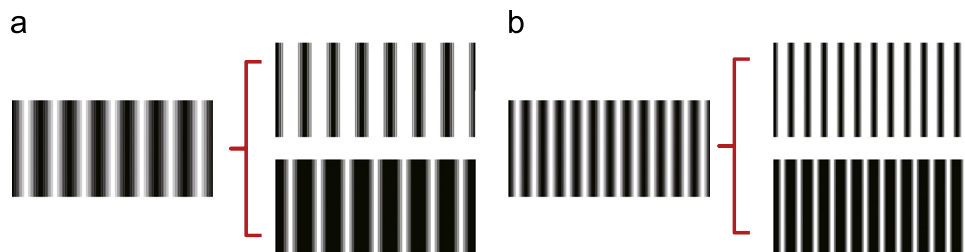
3. Experiments and results

Experiments with a high-speed 3-D fringe projection system was used to test the validity of the process described above in measuring the shape of static and moving objects having discontinuities and/or spatially isolated surfaces. The programmable projector used was a DLP LightCrafter DMD kit that which allows 4000 Hz binary pattern rate with a resolution of 608×684 and 50 lumens brightness. We used the configurable I/O trigger of the DLP LightCrafter for synchronizing with a high-speed camera (AOS X-PRI) which can capture 1250 fps with an 800×600 image resolution.

To determine the height of each point of the objects accurately, we employed a reference-plane based nonlinear phase-to-height mapping technique, described in detail in [36]. The relation between the phase and the height $z(x,y)$ can be written as

$$\frac{1}{z(x,y)} = a(x,y) + \frac{b(x,y)}{\Delta\Phi(x,y)} + \frac{c(x,y)}{\Delta\Phi^2(x,y)}, \tag{15}$$

where $\Delta\Phi(x,y)$ is the relative absolute phase from the reference plane. $a(x,y)$, $b(x,y)$, and $c(x,y)$ are the calibration parameters, which can be calculated from a standard flat plane sliding on a linear translation stage with four or more different distances.

3.1. Pattern projection and capture

To guarantee high measurement accuracy, the TPWM patterns have been carefully designed according to the optimization criterion proposed in [13]. For I_1–I_3, we chose the fringe pitch of 48 pixels and $f_c = 7f_0$, and for I_4–I_5, we chose the fringe pitch of 28 pixels and $f_c = 5f_0$. Therefore, the nonambiguous measurement range was 336 pixels, which was sufficient to guarantee that all the phase jumps in discontinuous surfaces and large step heights fall in this range.

To realize the tripolar pattern projection, we first decomposed each ternary patterns into two 1-bit pattern: for intensity 0, the corresponding pixel values in the two partitioned binary images were both zeros, for intensity 1, the corresponding pixel values in the two partitioned binary images were both ones, while for intensity 0.5, the value was 1 in the first binary image and was zero for the second one. The original TPWM patterns and their decomposed ones are shown in Fig. 4. After that, the ten binary images were projected sequentially and repeatedly by the DLP LightCrafter at the speed of 2500 fps. We properly controlled the camera trigger signal, guaranteeing that the exposure period of the camera straddles symmetrically the two partitioned binary images so that the three intensity level could be precisely reproduced. In our experiments, the camera was working at 1250 fps with the exposure time of 600 μs. So the trigger signal was delayed 100 μs after one pattern was projected. The timing signals of the system are illustrated in Fig. 5. A five-pattern sliding

Fig. 4. TPWM patterns and their decompositions. (a) Fringe pitch 48 pixels; (b) Fringe pitch 28 pixels.
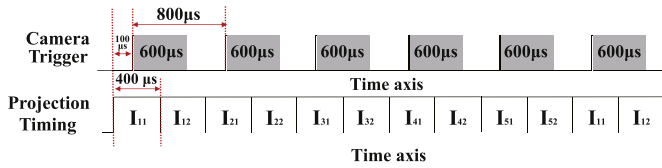
Fig. 5. Timing signals of the experimental system. The exposure period of the camera lasting 600 μs is shown by shaded gray region.
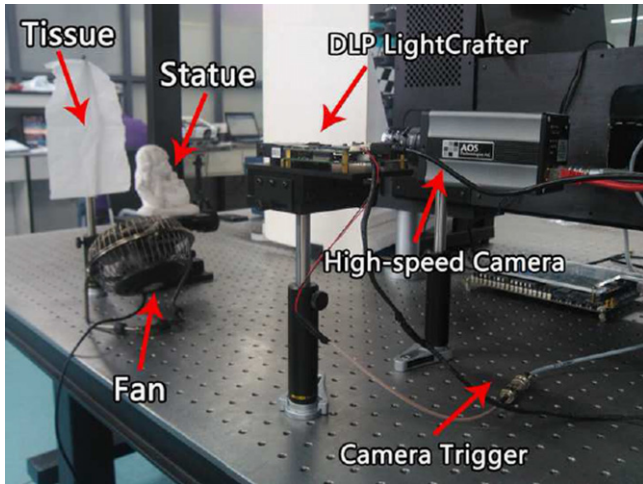

Fig. 6. Photograph of the measured scene and the high-speed 3-D shape measurement system.

window along the whole captured pattern sequence was applied, thus the acquisition speed of the 3-D data was also 1250 fps.

3.2. Scene I: static statue with a waving tissue.

In this experiment, we used a piece of tissue as a flag and fixed its one side on a pole. The tissue was then blown from the fixed side by a fan and to produce waves like a flag rippling in the wind. We also placed a static plaster statue separately on the right. A photograph of the waving flag is shown in Fig. 6. In Fig. 7(a)–(e), we show five captured fringe images, from which two unwrapped phase maps could be obtained simultaneously, shown in Fig. 7(f)–(g). After the weighted difference between the two phases was calculated, the entry for the LUT could be obtained, which are shown in Fig. 7(h). After phase-unwrapping, we got two the two absolute phases which are shown in Fig. 7(i) and (j). It can be observed that by using our bi-frequency phase-shifting method combining with the number-theoretical phase-unwrapping, two absolute phases can be recovered correctly. To demonstrate the phase-unwrapping process as well as how the phase error may affect the phase-unwrapping more clearly, in Fig. 7(k) we show the cross-sections of the $(p_2\phi_1 - p_1\phi_2)/2\pi$ (without rounding to the nearest integer) along one row highlighted in Fig. 7(h). The ideal values are also plotted. It can be seen that, although the measured values contained some noise, they could be rounded to the correct integer without error. The steps in Fig. 7(k) exhibits different heights, therefore (k_1, k_2) could be determined uniquely and hence the absolute phase Φ_1 and Φ_2 could be recovered without ambiguity. To examine the phase noise more clearly, we plot one row of the error signal between the ideal stair image and the calculated one in Fig. 7(l). It is
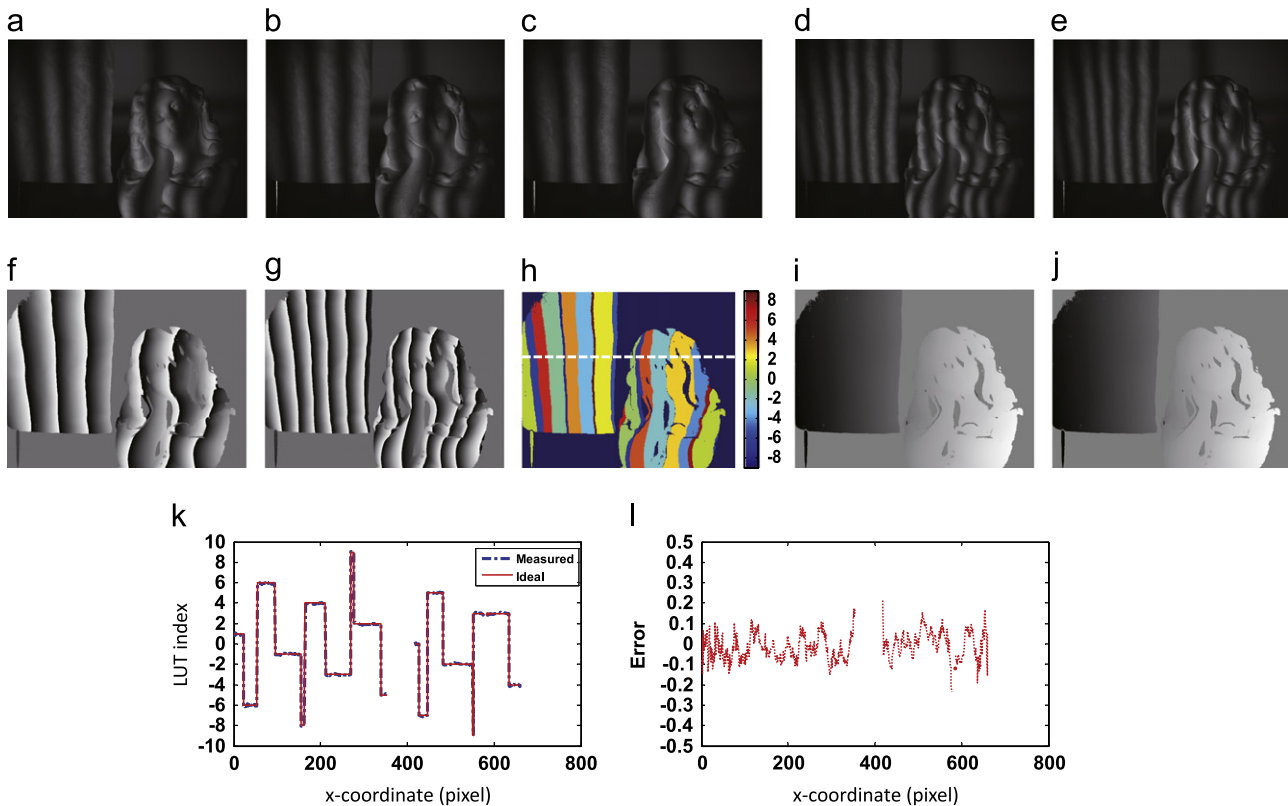

Fig. 7. (a)–(e) Captured scene with fringe patterns; (f) wrapped phase map 1 (fringe pitch 48 pixels); (g) wrapped phase map 2 (fringe pitch 28 pixels); (h) the segmented regions identified by the rounded $(p_2\phi_1 - p_1\phi_2)/2\pi$ for the LUT; (i) absolute phase map 1(fringe pitch 48 pixels); (g) absolute phase map 2 (fringe pitch 28 pixels); (k) one cross-section (highlighted in (h)) of the measured $(p_2\phi_1 - p_1\phi_2)/2\pi$ and its corresponding ideal values; (f) error signal between the ideal stair signal and the calculated one.

obvious that the maximal error did not exceed 0.5, so the absolute phase maps were recovered from the wrapped ones free from fringe order misrecognition.

With the absolute phase obtained, along with the calibration parameters, the final 3-D data could be calculated. We present the video of measurement results in slow play (100 fps). Fig. 8(a) shows one frame of the reconstructed 3-D result with color-coded depth. Red represents near objects, and blue, far objects. By averaging the three fringe patterns with 48 pixels wavelength, the texture of the objects could be obtained as well. Fig. 8(b) shows the texture rendered 3-D result from another viewpoint. Even when the objects are isolated, in motion, and moreover, have pronounced variations in surface conditions such as convex and concave curvatures, no irregularities are recognizable in the final results (Video 1), which verified the success of the proposed method in simultaneously measuring multiple moving objects.

3.3. Scene II: a rotating fan

The second test scene contained a small desk fan with three blades each measuring 5.5 cm in the radial direction out from the center hub which has a diameter of 3.5 cm. The desk fan was rotated at a slow speed about 300 rotations per minute (RPM). Fig. 9(a) shows the appearance of the fan. Fig. 9(b) shows one captured fringe image of the fan. Since the rotation speed is comparable to the time required for measurements, some unreliable results emerged, especially around the edges of the fan blades. These outliers can be automatically removed by the use the algorithm in Ref. [37]. One frame of final reconstructed data is shown in Fig. 9(c) and the resultant movie is presented in Video. 2, replayed in only 1/50 of the capturing rate (25 fps). The results clearly show that the proposed method can faithfully reconstruct 3-D shapes of moving object with discontinuities and large depth variations.
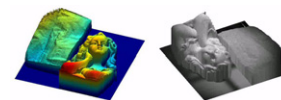
4. Conclusions and discussions

A novel high-speed three-dimensional shape measurement technique for recovering absolute phase and measuring spatially isolated objects under dynamic conditions has been presented. This method employs only five bi-frequency phase-shifted sinusoidal patterns to calculate two different unwrapped phase maps. Using a two-frequency number-theoretical approach, the two phase maps can be unwrapped on a pixel-by-pixel basis without ambiguities. To achieve high-speed, accurate pattern projection, TPWM technique is employed which could produce close-to-ideal sinusoidal patterns with slight defocus. Experimental results on dynamic scenes show that the technique can reliably obtain shape and texture information of moving objects at a rate of 1250 fps.

It is also worth mentioning that in this work we assume that the camera does not induce any response nonlinearity so that the gray-tone of the quasi-ideal projected pattern can be faithfully reproduced without distortion. In the case when the camera response is not perfect linear, extra error will induced, affecting the precision of phase-unwrapping and the final measurements. Perhaps the only way to elude the nonlinearity problem of the camera is to use binary coding and decoding [38,39]. As both the projected patterns and the acquired images are binarized, non-linear response of the projector and the camera will not play a role. However, since depth information can be carried with only two levels, a greater number of frames are required. Although the frame number can be reduced by color encoding, it is helpless to reduce the measurement time for high-speed (kHz) applications since the DMD is a binary digital device and the color images are separated into their RGB components for sequential display. Human eyes or a low-speed camera cannot 'see' this process because the colors are switched at a sufficiently high rate. Besides, the binarization may be difficult to implement when the image blur, and the color coupling and imbalance exist. Perhaps the simplest way to avoid this problem is to try to make the camera response linearly by changing its settings, e.g. turn off the functions like 'gamma-correction' and 'automatic gain control (AGC)' function. In that case, nonlinearity of the camera can be neglected compared to that of the projector.

In conclusion, the method proposed in this work has the advantages of high-speed, high-precision, non-ambiguity, and full-field for 3-D data acquisition and analysis, rendering it a promising technique of dynamic 3-D shape measurement of multiples objects with complex shapes. Besides, the detailed explanations about the principle and implementation of proposed method may also provide a nice technical guide for someone planning high speed profilometry in engineering applications.

Video 1. Real-time measurement of a complex scene, the result is shown with color-coded depth (left) and texture (right). (QuickTime, 4.62 MB). A video clip is available online. Supplementary material related to this article can be found online at http://dx.doi.org/10.1016/j.optlaseng.2013.02.012.
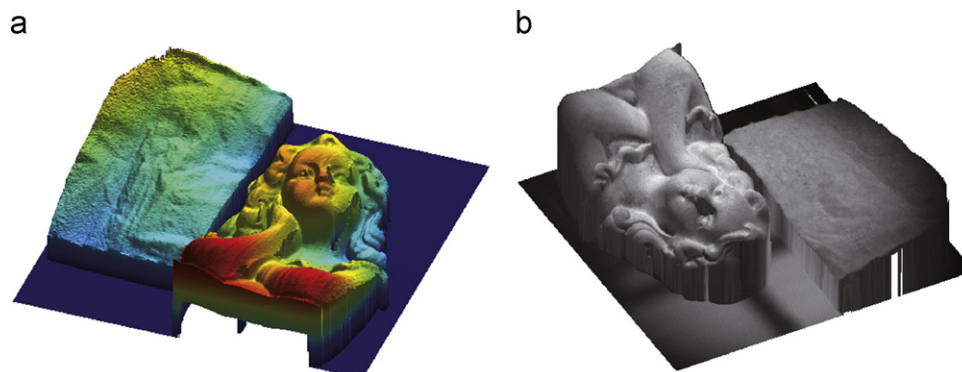

Fig. 8. Reconstructed 3-D result with color-coded depth (a) and texture (b).
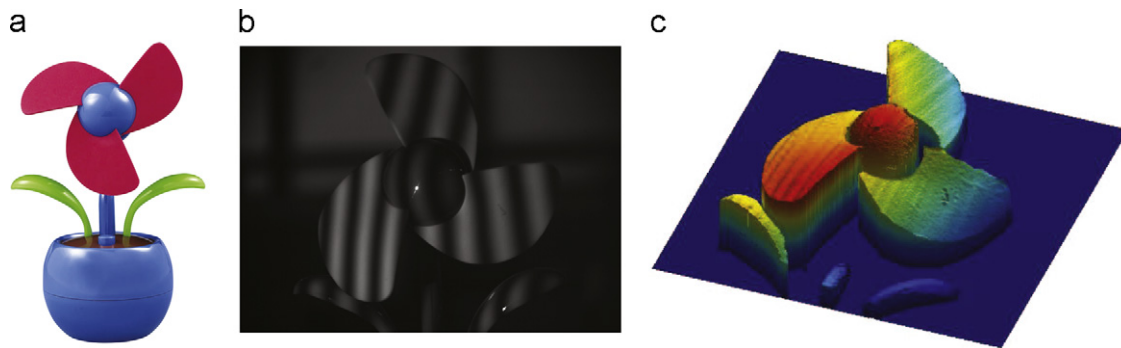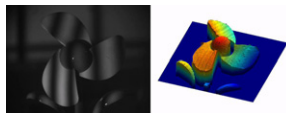
Fig. 9. Measurement result of a rotating fan. (a) Photograph of the measured fan; (b) one captured fringe image of the fan; (c) the reconstructed 3-D result.

Video 2. . Real-time measurement result of a rotating fan, left half shows the fringe patterns captured, right half shows the reconstructed 3-D result (Quick-Time, 3.68 MB). A video clip is available online. Supplementary material related to this article can be found online at http://dx.doi.org/10.1016/j.optlaseng.2013.02.012.

Acknowledgments

References

[1] Chen F, Brown GM, Song MM. Overview of three-dimensional shape measurement using optical methods. Opt Eng 2000;39:10–22.
[2] Gorthi SS, Rastogi P. Fringe projection techniques: whither we are? Opt Laser Eng 2010;48:133–40.
[3] Su XY, Zhang QC. Dynamic 3-D shape measurement method: a review. Opt Laser Eng 2010;48:191–204.
[4] Zhang S. Recent progresses on real-time 3D shape measurement using digital fringe projection techniques. Opt Laser Eng 2010;48:149–58.
[5] Gong Y, Zhang S. Ultrafast 3-D shape measurement with an off-the-shelf DLP projector. Opt Express 2010;18:19743–54.
[6] Zhang Q, Su X. High-speed optical measurement for the drumhead vibration. Opt Express 2005;13:3110–6.
[7] Zhang S, Van Der Weide D, Oliver J. Superfast phase-shifting method for 3-D shape measurement. Opt Express 2010;18:9684–9.
[8] Zhang S. Composite phase-shifting algorithm for absolute phase measurement. Opt Laser Eng 2012;50:1538–41.
[9] Zhang ZH. Review of single-shot 3D shape measurement by phase calculation-based fringe projection techniques. Opt Laser Eng 2012;50:1097–1106.
[10] Zhang S, Huang PS. High-resolution, real-time three-dimensional shape measurement. Opt Eng 2006;45:123601–8.
[11] Huang PSS, Zhang CP, Chiang FP. High-speed 3-D shape measurement based on digital fringe projection. Opt Eng 2003;42:163–8.
[12] Weise T, Leibe B, Van Gool L. Fast 3D scanning with automatic motion compensation. IEEE Conference on computer vision and pattern recognition. CVPR 07; 2007. p. 1–8.
[13] Zuo C, Chen Q, Gu G, Feng S, Feng F. High-speed three-dimensional profilometry for multiple objects with complex shapes. Opt. Express 2012;20:19493–510.
[14] Wang YJ, Zhang S. Optimal pulse width modulation for sinusoidal fringe generation with projector defocusing. Opt Lett 2010;35:4121–3.
[15] Wang YJ, Zhang S, Oliver JH. 3D shape measurement technique for multiple rapidly moving objects. Opt Express 2011;19:8539–45.
[16] Zuo C, Chen Q, Feng SJ, Feng F, Gu GH, Sui XB. Optimized pulse width modulation pattern strategy for three-dimensional profilometry with projector defocusing. Appl Opt 2012;51:4477–90.
[17] Lei SY, Zhang S. Flexible 3-D shape measurement using projector defocusing. Opt Lett 2009;34:3080–2.
[18] Ayubi GA, Ayubi JA, Di Martino JM, Ferrari JA. Pulse-width modulation in defocused three-dimensional fringe projection. Opt Lett 2010;35:3682–4.
[19] Wang Y, Zhang S. Comparison of the squared binary, sinusoidal pulse width modulation, and optimal pulse width modulation methods for three-dimensional shape measurement with projector defocusing. Appl Opt 2012;51:861–72.
[20] Zhang S, Van Der Weide D, Oliver J. Superfast phase-shifting method for 3-D shape measurement. Opt Express 2010;18:9684–9.
[21] Wang YJ, Zhang S. Superfast multifrequency phase-shifting technique with optimal pulse width modulation. Opt Express 2011;19:5149–55.
[22] Sansoni G, Carocci M, Rodella R. Three-dimensional vision based on a combination of gray-code and phase-shift light projection: analysis and compensation of the systematic errors. Appl Opt 1999;38:6565–73.
[23] Zhang Q, Su X, Xiang L, Sun X. 3-D shape measurement based on complementary gray-code light. Opt Laser Eng 2012;50:574–9.
[24] Li JL, Hassebrook LG, Guan C. Optimized two-frequency phase-measuring-profilometry light-sensor temporal-noise sensitivity. J Opt Soc Am A 2003;20:106–15.
[25] Huntley JM, Saldner HO. Shape measurement by temporal phase unwrapping and spatial light modulator-based fringe projector. Proc SPIE 1997;3100:185–192.
[26] Judge TR, Bryanston-Cross PJ. A review of phase unwrapping techniques in fringe analysis. Opt Laser Eng 1994;21:199–239.
[27] Creath K. Step height measurement using two-wavelength phase-shifting interferometry. Appl Opt 1987;26:2810–6.
[28] Towers CE, Towers DP, Jones JDC. Optimum frequency selection in multi-frequency interferometry. Opt Lett 2003;28:887–9.
[29] Zhang ZH, Towers CE, Towers DP. Time efficient color fringe projection system for 3D shape and color using optimum 3-frequency selection. Opt Express 2006;14:6444–55.
[30] Zhong JG, Zhang YL. Absolute phase-measurement technique based on number theory in multifrequency grating projection profilometry. Appl Opt 2001;40:492–500.
[31] Towers CE, Towers DP, Jones JDC. Time efficient Chinese remainder theorem algorithm for full-field fringe phase analysis in multi-wavelength interferometry. Opt Express 2004;12:1136–43.
[32] Lilienblum E, Michaelis B. Optical 3D surface reconstruction by a multi-period phase shift method; 2007.
[33] Ding Y, Xi JT, Yu YG, Chicharo J. Recovering the absolute phase maps of two fringe patterns with selected frequencies. Opt Lett 2011;36:2518–20.
[34] Ding Y, Xi JT, Yu YG, Cheng WQ, Wang S, Chicharo JF. Frequency selection in absolute phase maps recovery with two frequency projection fringes. Opt Express 2012;20:13238–51.
[35] Rosen KH. Elementary number theory and its applications. Addison-Wesley publishing Co.; 1988.
[36] Li W, Su X, Liu Z. Large-scale three-dimensional object measurement: a practical coordinate mapping and image data-patching method. Appl Opt 2001;40:3326–33.
[37] Feng S, Chen Q, Zuo C, Li R, Shen G, Feng F. Automatic identification and removal of outliers for high-speed fringe projection profilometry. Opt Eng 2013;52:013605–013605, http://dx.doi.org/10.1117/1.OE.52.1.013605.
[38] Ayubi GA, Di Martino JM, Alonso JR, Fernández A, Flores JL, Ferrari JA. Color encoding of binary fringes for gamma correction in 3-D profiling. Opt Lett 2012;37:1325–7.
[39] Ayubi GA, Di Martino JM, Flores JL, Ferrari JA. Binary coded linear fringes for three-dimensional shape profiling. Opt Eng 2012;51 103601-103601.